Numerical simulation of the transverse hydrogen injection into a supersonic turbulent airstream

Yekaterina Moisseyeva Altynshash Naimanova
K.Moisseyeva@gmail.com

Abstract

Three-dimensional turbulent steady flowfield generated by transverse hydrogen injection into a supersonic cross-flow was simulated by solving the Reynolds-averaged Navier-Stokes equations using the ENO scheme. Analysis of different variations of the limiter functions for developed algorithm was done to define the optimal function producing the smallest spread of solution. The effect of the limiter choice on the mixing layer dynamics was studied. It was shown that choice of some limiters can result in excessive expansion of the mixing layer, that is important for numerical modeling of scramjet engine.

1 Introduction

Currently, in numerical simulations of supersonic flows the main tool is the essentially non-oscillating schemes: ENO (essentially non-oscillatory) and WENO (weighted essentially non-oscillatory) schemes. These schemes are well adapted for solving the Navier-Stokes equations for a perfect gas [3, 2, 1]. Multicomponent gas flow modeling is important for practical application, but these schemes are less adapted for such problems. The ENO scheme based on the Godunov method was developed and its applicability to the problem of transverse jet injection into a supersonic turbulent multicomponent gas flow in a flat channel was shown by the authors in [4].

As well known, piece-wise function distribution inside a cell is used during construction of high-order methods in space. To define the function on the cell boundary by its value in the cell center it is necessary to introduce a reconstruction procedure. Conditions imposed on the function slope is modified by limiters. In this case, the main difficulty is related with ambiguity of the choice of these functions. Most of the research on the effect of limiter choice on the solution has been in one dimensions [5, 6]. Different ways of reconstruction in two and three dimension are set out in [7, 8]. It should be noticed that multidimensional reconstructions do not have strict justification. Applicability of these methods should be investigated in every particular case.

The aim of this paper is numerical modeling of a three-dimensional turbulent steady flowfield generated by transverse hydrogen injection into a supersonic cross-flow (Fig.1). To solve this problem, numerical method developed by authors in [4], based on the third order ENO scheme is adapted for three-dimensional case. Additionally, the effective adiabatic parameter of the gas mixture is introduced. It allows one to calculate the derivatives of the pressure with respect to independent variables for determining the Jacobian matrices, and thus to construct an efficient implicit algorithm of the solution. Effect of the limiter choice in numerical algorithms on the mixing layer is studied since the exact calculation of the mass concentration spread is an important issue in combustion problem modeling.

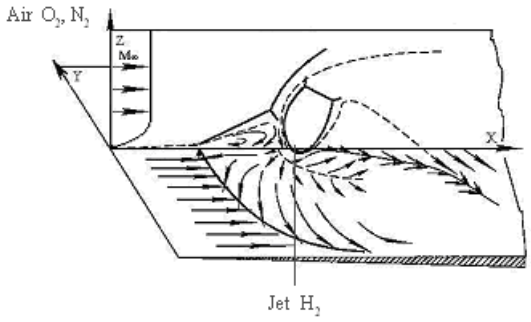

Figure 1: Schematics of flowfield

Also the mechanism of the formation of vortices in front of the injected jet and behind that is studied.

2 Problem formulation

Basic equations for the problem are the system of the three-dimensional Reynolds averaged Navier-Stokes equations for the compressible turbulent multicomponent gas in the Cartesian coordinate system written in conservative form as

$$\frac{\partial \underline{U}}{\partial t} + \frac{\partial \left(\underline{E} - \underline{E}_v\right)}{\partial x} + \frac{\partial \left(\underline{F} - \underline{F}_v\right)}{\partial y} + \frac{\partial \left(\underline{G} - \underline{G}_v\right)}{\partial z} = 0, \tag{1}$$

$$\underline{U} = \left(\rho, \rho u, \rho v, \rho w, E_t, \rho Y_k\right)^T, \underline{E} = \left(\rho u, \rho u^2 + p, \rho uv, \rho uw, \left(E_t + p\right) u, \rho u Y_k\right)^T,$$

$$\underline{F} = \left(\rho v, \rho uv, \rho v^2 + p, \rho vw, \left(E_t + p\right) v, \rho v Y_k\right)^T,$$

$$\underline{G} = \left(\rho w, \rho uw, \rho vw, \rho w^2 + p, \left(E_t + p\right) w, \rho w Y_k\right)^T,$$

$\underline{E}_v, \underline{F}_v, \underline{G}_v$ vectors are associated with viscous stress

$$\underline{E}_v = \left(0, \tau_{xx}, \tau_{xy}, \tau_{xz}, u\tau_{xx} + v\tau_{xy} + w\tau_{xz} - q_x, J_{kx}\right)^T,$$

$$\underline{F}_v = \left(0, \tau_{xy}, \tau_{yy}, \tau_{yz}, u\tau_{xy} + v\tau_{yy} + w\tau_{yz} - q_y, J_{ky}\right)^T,$$

$$\underline{G}_v = \left(0, \tau_{xz}, \tau_{yz}, \tau_{zz}, u\tau_{xz} + v\tau_{yz} + w\tau_{zz} - q_z, J_{kz}\right)^T,$$

where $\tau, \underline{q}$ and $\underline{J_k}$ are viscous stress tensor, heat flux and diffusion flux, respectively.

Pressure and total energy are defined by

$$p = \frac{\rho T}{\gamma_\infty M_\infty^2} \sum_{k=1}^{N} \frac{Y_k}{W_k}, \; E_t = \frac{\rho}{\gamma_\infty M_\infty^2} \sum_{k=1}^{N} Y_k h_k - p + \frac{1}{2}\rho(u^2 + v^2 + w^2)$$

Viscosity coefficient is defined as a sum of laminar and turbulent viscosity coefficients: $\mu = \mu_l + \mu_t$, where μ_l is determined by Wilke formula, and μ_t is determined by $k - \omega$ turbulent model [9].

In the system (1) u, v, w, ρ, T represent components of velocity vector, density and temperature, respectively. Y_k, W_k and h_k are mass fraction, molecular weight and specific enthalpy of the kth species, where Y_1 stands for mass fraction of H_2, Y_2 for mass fraction

of O_2, Y_3 for mass fraction of N_2. γ is adiabatic parameter, M is Mach number. Index 0 indicates jet parameters and index ∞ indicates parameters of the main flow.

The system (1) is written in a nondimensional form. Constitutive parameters are parameters of the main flow at the inlet ($u_\infty,\ \rho_\infty,\ T_\infty$). The injector diameter d is chosen as the characteristic length.

Boundary conditions. On the flow field entrance, the parameters of the free stream are given

$p = p_\infty,\ T = T_\infty,\ u = M_\infty\sqrt{\frac{\gamma_\infty R_0 T_\infty}{W_\infty}},\ v = w = 0,\ Y_k = Y_{k\infty},\ W_k = W_{k\infty},\ x = 0,\ 0 \le y \le H_y,\ 0 \le z \le H_z$.

Also boundary layer is given near the wall, longitudinal velocity component is approximated by 1/7th power law.

On the injector, parameters of the jet are given

$p = np_\infty,\ T = T_0,\ u = v = 0,\ w = M_0\sqrt{\frac{\gamma_0 R_0 T_0}{W_0}},\ Y_k = Y_{k0},\ W_k = W_{k0},\ z = 0,\ |x^2 + y^2| \le R$,

where n is the pressure ratio. The non-reflecting boundary conditions are adopted on the flow field exit. The adiabatic no-slip boundary condition on the wall and the symmetry boundary condition on the symmetry faces are specified. Here $H_x,\ H_y$ and H_z are the length, width and height of the computational domain, respectively. R is the injector radius.

3 Method of solution

In the regions of large gradients (in the boundary layer, near the wall and on the jet exit) condensation of the grid is introduced. Then the system (1) in the transformed coordinate system may be written as

$$\frac{\partial \tilde{U}}{\partial t} + \frac{\partial \tilde{E}}{\partial \xi} + \frac{\partial \tilde{F}}{\partial \eta} + \frac{\partial \tilde{G}}{\partial \zeta} = \frac{\partial \tilde{E}_{v2}}{\partial \xi} + \frac{\partial \tilde{E}_{vm}}{\partial \xi} + \frac{\partial \tilde{F}_{v2}}{\partial \eta} + \frac{\partial \tilde{F}_{vm}}{\partial \eta} + \frac{\partial \tilde{G}_{v2}}{\partial \zeta} + \frac{\partial \tilde{G}_{vm}}{\partial \zeta} \tag{2}$$

where $\tilde{U} = \left(\frac{1}{J}\right)\underline{U},\ \tilde{E} = \left(\frac{\xi_x}{J}\right)\underline{E},\ \tilde{F} = \left(\frac{\eta_y}{J}\right)\underline{F},\ \tilde{G} = \left(\frac{\zeta_z}{J}\right)\underline{G},\ \tilde{E}_{v2} = \left(\frac{\xi_x}{J}\right)\underline{E}_{v2},$

$\tilde{F}_{v2} = \left(\frac{\eta_y}{J}\right)\underline{F}_{v2},\ \tilde{G}_{v2} = \left(\frac{\zeta_z}{J}\right)\underline{G}_{v2},\ \tilde{E}_{vm} = \left(\frac{\xi_x}{J}\right)\underline{E}_{vm},\ \tilde{F}_{vm} = \left(\frac{\eta_y}{J}\right)\underline{F}_{vm},$

$\tilde{G}_{vm} = \left(\frac{\zeta_z}{J}\right)\underline{G}_{vm}$. $J = \frac{\partial(\xi,\eta,\zeta)}{\partial(x,y,z)}$ is the Jacobian of the transformation.

The diffusion terms are represented by the sum of second derivative terms (which indicated by index $v2$) and mixed derivative terms (which indicated by index vm).

For numerical solution of the system (2) ENO scheme of the third order is used for spatial discretization. Method of numerical algorithm construction was shown in [4]. In accordance with the principle of the ENO scheme, the one-step finite difference scheme for the time integration of the system (2) is presented formally as

$$\Delta\tilde{U}^{n+1} + \Delta t\left\{\left(\hat{A}^+ + \hat{A}^-\right)\frac{\partial \underline{E}^m}{\partial \xi} + \left(\hat{B}^+ + \hat{B}^-\right)\frac{\partial \underline{F}^m}{\partial \eta} + \left(\hat{C}^+ + \hat{C}^-\right)\frac{\partial \underline{G}^m}{\partial \zeta} - \right.$$
$$\left. - \left[\frac{\partial\left(\tilde{E}_{v2}^{n+1} + \tilde{E}_{vm}^{n}\right)}{\partial \xi} + \frac{\partial\left(\tilde{F}_{v2}^{n+1} + \tilde{F}_{vm}^{n}\right)}{\partial \eta} + \frac{\partial\left(\tilde{G}_{v2}^{n+1} + \tilde{G}_{vm}^{n}\right)}{\partial \zeta}\right]\right\} = O\left(\frac{1}{2}\Delta t^2\right) \tag{3}$$

Here $\underline{E}^m$, $\underline{F}^m$, $\underline{G}^m$ are the modified fluxes at the node point (i,j,k), which consist of the original convective vectors ($\tilde{E}$, $\tilde{F}$, $\tilde{G}$) and additional terms of the high order of accuracy ($\underline{E}_\xi, \underline{D}_\xi$, $\underline{E}_\eta, \underline{D}_\eta$, $\underline{E}_\zeta, \underline{D}_\zeta$):

$$\underline{E}^m = \tilde{E}^{n+1} + \left(\underline{E}_\xi + \underline{D}_\xi\right)^n,$$

where $\underline{E}_{\xi ijk} = limiter1(\bar{E}_{\xi i-1/2jk},\ \bar{E}_{\xi i+1/2jk})$

$$\underline{D}_{\xi ijk} = \begin{cases} limiter2(\Delta_-\hat{D}_{\xi i-1/2jk},\ \Delta_+\hat{D}_{\xi i-1/2jk}) & \text{if } \left|\Delta_-\tilde{U}_{ijk}\right| \le \left|\Delta_+\tilde{U}_{ijk}\right| \\ limiter2(\Delta_-\bar{D}_{\xi i+1/2jk},\ \Delta_+\bar{D}_{\xi i+1/2jk}) & \text{if } \left|\Delta_-\tilde{U}_{ijk}\right| > \left|\Delta_+\tilde{U}_{ijk}\right| \end{cases} \text{for } \lambda > 0$$

$$\underline{D}_{\xi ijk} = \begin{cases} limiter2(\Delta_-\bar{D}_{\xi i-1/2jk},\ \Delta_+\bar{D}_{\xi i-1/2jk}) & \text{if } \left|\Delta_-\tilde{U}_{ijk}\right| \le \left|\Delta_+\tilde{U}_{ijk}\right| \\ limiter2(\Delta_-\hat{D}_{\xi i+1/2jk},\ \Delta_+\hat{D}_{\xi i+1/2jk}) & \text{if } \left|\Delta_-\tilde{U}_{ijk}\right| > \left|\Delta_+\tilde{U}_{ijk}\right| \end{cases} \text{for } \lambda \le 0$$

where $\bar{E}_{\xi i+1/2jk} = \frac{1}{2} sign(A_{i+1/2jk}) \left(I - \frac{\Delta t}{\Delta \xi}\left|A_{i+1/2jk}\right|\right)$

$$\bar{D}_{\xi i+1/2jk} = \frac{1}{6} sign(A_{i+1/2jk}) \left[\left(\frac{\Delta t}{\Delta \xi}\left|A_{i+1/2jk}\right|\right)^2 - I\right]$$

$$\hat{D}_{\xi i+1/2jk} = \frac{1}{6} sign(A_{i+1/2jk}) \left[2I - 3\frac{\Delta t}{\Delta \xi}\left|A_{i+1/2jk}\right| + \left(\frac{\Delta t}{\Delta \xi}\left|A_{i+1/2jk}\right|\right)^2\right]$$

$\hat{A}^\pm = A^\pm/A$ and $\hat{A}^+ + \hat{A}^- = I$, $A^\pm = R\Lambda^\pm R^{-1} = R\left(\frac{\Lambda \pm |\Lambda|}{2}\right)R^{-1}$.

I is the identity matrix, $A = \partial\underline{E}/\partial\underline{U}$ is the Jacobi matrix.

Here the limiter functions $limiter1(a,b)$ and $limiter2(a,b)$ are associated with the terms of the second and third order of accuracy, respectively. Functions $m(a,b)$, $minmod(a,b)$ or $superbee(a,b)$ are chosen as limiters, where

$$limiter1(a,b) = \dot{m}(a,b) = \begin{cases} \frac{1}{2}a & \text{if } |a| \le |b| \\ \frac{1}{2}b & \text{if } |a| > |b| \end{cases}$$

$$limiter1(a,b) = minmod(a,b) = \begin{cases} s \cdot min(|a|,|b|) & \text{if } sign(a) = sign(b) = s \\ 0 & \text{else} \end{cases} \quad (4)$$

$$limiter1(a,b) = superbee(a,b) = \begin{cases} \begin{cases} min(2a,b) & \text{if } |a| \le |b| \\ min(a,2b) & \text{if } |a| > |b| \end{cases} & \text{if } sign(a) = sign(b) \\ 0 & \text{else} \end{cases}$$

$limiter2(a,b)$ is determined in the same way, and the expressions for the fluxes $\underline{F}^m$ and $\underline{G}^m$ are written similarly to $\underline{E}^m$.

Numerical solution of the system (3) is performed in two steps. At the first step thermodynamic parameters ρ, u, v, w, E_t and at the second step mass fractions Y_k are resolved. The upwind differences of the first order of accuracy have been used for the approximation of the first derivatives in the system (3), and the central differences of the second order of accuracy have been used for the second derivatives. The obtained system of equations is solved with respect to the vector of thermodynamic parameters by the matrix sweep method, and the vector of mass fractions of the mixture is computed by tridiagonal inversion.

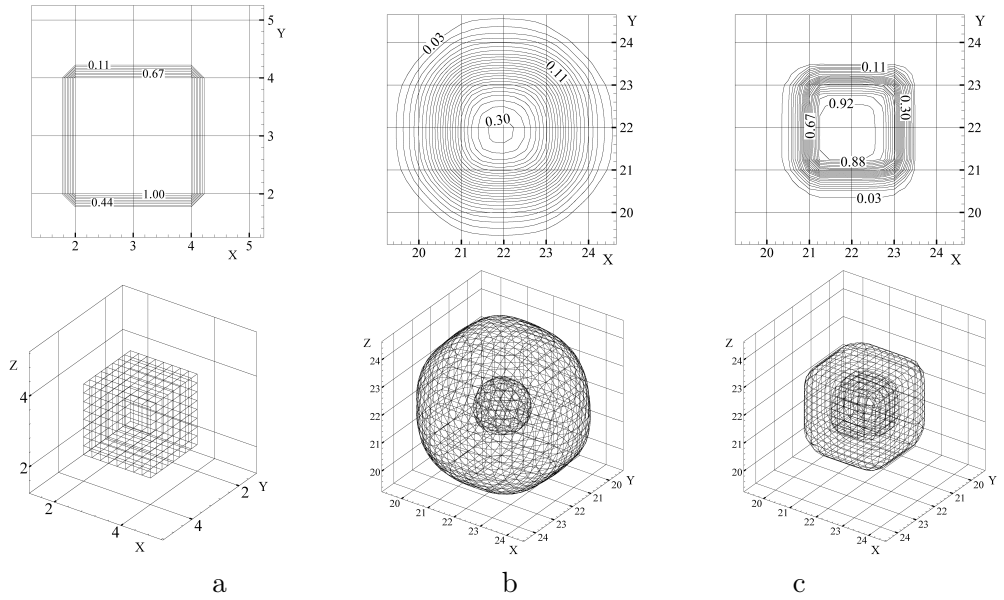

Figure 2: Numerical solution of substance balance equation: a - initial distribution, b, c - distribution at the time moment $t = 19$ for the limiters (5aa) and (5b), respectively.

4 Results

As was indicated in introduction, the choice of the limiter function significantly affects the accuracy of the problem. So, preliminarily test problem of hydrogen mass fraction transfer was solved to validate numerical method and choose optimal limiter. The velocities are regarded as constant and equal to 1. Initial condition for the hydrogen mass fraction is given as cube cloud of lenth 2 (Fig.2a).

The limiters function were chosen from (4) as

$$limiter1(a,b) = minmod(a,b),\ limiter2(a,b,) = \dot{m}(a,b); \tag{5a}$$

$$limiter1(a,b) = 1.1superbee(a,b),\ limiter2(a,b) = \dot{m}(a,b) \tag{5b}$$

It follows from Fig.2b that the solution obtained with (5aa) significantly spreads the original solution, i.e. the limiter (5aa) reduces dissipative effects insufficiently. The original shape of the cube is not preserved. The cloud becomes a symmetrical sphere at the time moment $t = 19$. On the contrary, slight change of the second order limiter (5b) brings about significant reduce of dissipative effects. The cube cloud preserves its shape. Slight spread of the solution at the time moment $t = 19$ occurs (Fig.2c).

The numerical computations of the original problem (1) were done on the staggered spatial grid $101 \times 81 \times 81$ with the parameters: time step $\Delta t = 0.01$, $Pr = 0.9$, $M_0 = 1$, $M_\infty = 4$, $4 \le n \le 15$, $Re = 10^4$; $H_x = 20$, $H_y = 15$, $H_z = 10$ calibres, $x_0 = 10$ calibres is distance from entrance boundary to injector center.

The flowfield without hydrogen jet is computed first to validate the reliability of the numerical method with the following freestream parameters from the experiment by [10]: $M_\infty = 4$, $T_\infty = 376.8\ K$, $Re = 6.1 \times 10^7$. The obtained velocity profile in the turbulent boundary layer is given in Fig. 3. It can be seen that the velocity profile well agree with the experimental data, that indicates the reliability of the numerical scheme and the turbulence model.

Thereafter, the flowfield with the hydrogen jet is simulated using different limiters (5). Since accurate computation of mass fraction distribution is an important issue for

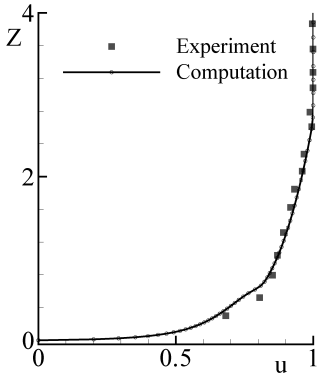

Figure 3: Velocity profile in turbulent boundary layer

combustion modeling, Figs. 4 and 5 give distribution of the hydrogen mass fraction in the symmetry section XZ and in the different sections YZ, respectively. Here, the results obtained by making use of the limiters (5*a*a) are shown on the left, and the results for (5*b*) are shown on the right. It can be seen that spreading of the solution is well observable by the regions of the maximum and minimum values ($Y_1 = 0.99,\ Y_1 = 0.01$).

According to the comparison of Figs. 4 and 5, jet expansion in XZ is considerably less than that in YZ. It occurs because of the great drift of the injected substance by the main flow. Also it can be noticed that making use of (5*a*a) brings about a significant increase of the solution spreading. Thus, the maximum value of height for 1% hydrogen concentration is $z_{max} = 3.51$ for (5*a*a) and $z_{max} = 2.95$ for (5*b*).

Fig.5a-b shows that hydrogen penetration in the region in front of the jet spreads insignificantly near the wall, ie in subsonic region. Noticeable lateral jet expansion in the injector center (Fig.5c-d) is obviously due to the presence of lateral vortices leading to the main flow velocity reduce. Accumulation of the injected substance occurs behind the jet,then it decreases downstream (Fig.5e-f). In the transverse sections, significant solution spreading is also can be seen for (5*a*a) in comparison with the results for (5*b*).

5 Conclusion

The numerical method of the Reynolds averaged Navier-Stokes equations for multispecies gas flow solution developed by the authors in [4], based on the third order ENO scheme is adapted for the three-dimensional case. Different variations of the limiter functions were analysed for the developed algorithm. By numerical experiments the effect of the limiters on the shock-wave structure formation and on the mixing layer was studied. It

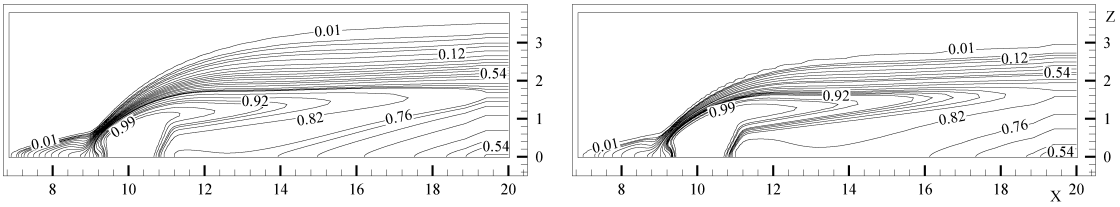

a b

Figure 4: Distribution of the hydrogen mass fraction in the symmetry section XZ for the limiter functions (5*a*a) (a) and (5*b*) (b)

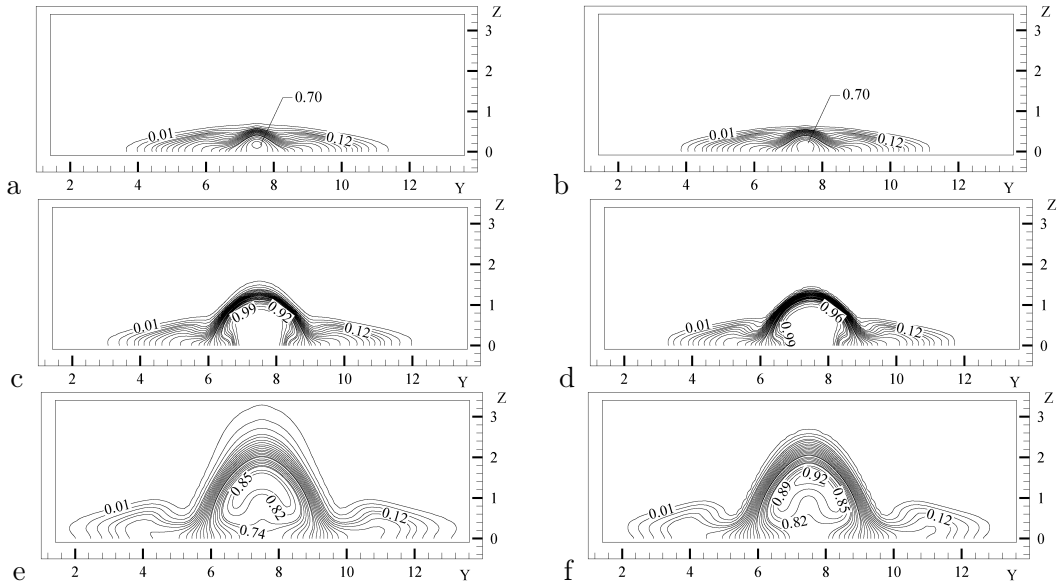

Figure 5: Distribution of the hydrogen mass fraction in the different sections YZ: at $x/d = 9.06$ with (5aa) (a) and (5b) (b); at $x/d = 10.0$ with (5aa) (c) and (5b) (d); at $x/d = 15.33$ with (5aa) (e) and (5b) (f).

was obtained that the choice of some limiters can result in the excessive expansion of the mixing layer, which is the important issue in numerical modeling of the scramjet engine. As result, the optimal function which produces the smallest spread of the solution for the spatial problem was defined.

References

[1] Adams N.A., Shariff K. A High-Resolution Hybrid Compact-ENO Scheme for Shock-Turbulence Interaction Problems // Journal of Computational Physics, Volume 127, Issue 1, August 1996, pp. 27в Ъ“51

[2] Sun De-chuan, Hu Chun-bo, Cai Ti-min. Computation of Supersonic Turbulent Flowfield with Transverse Injection // Applied Mathematics and Mechanics. English Edition. Vol.23, No 1, Jan 2002. pp. 107-113

[3] Amano R.S., Sun D. Numerical Simulation of Supersonic Flowfield with Secondary Injection // The 24th Congress of ICAS, September 2004, Yokohama.

[4] Bruel P., Naimanova A. Zh. Computation of the normal injection of a hydrogen jet into a supersonic air flow // Thermophysics and Aeromechanics, Vol. 17 issue 4 December 2010. pp. 531в Ъ“542

[5] Harten A. High resolution schemes for hyperbolic conservation laws // J. Comp. Phys., Vol. 49, 1983, pp. 357-393

[6] Harten A., Engquist B., Osher S., Chakravarthy S. Uniformly high-order accurate essentially non-oscillatory schemes III // J. Comput. Phys., Vol. 71, 1987, pp. 231-303

[7] Shu C., Osher S. Efficient Implementation of Essentially Non-Oscillatory Shock-Capturing Schemes, II // J. Comp. Phys., Vol. 83, 1989, pp. 32-78.

[8] Berger M.J., Aftosmis M.J., Murman S.E. Analysis of slope limiters on irregular grids // In 43rd AIAA Aerospace Sciences Meeting, Reno, NV , 2005. Paper AIAA 2005-0490.

[9] Rumsey C L. Compressibility considerations for $k-\omega$ turbulence models in hypersonic boundary layer applications. NASA/TM-2009-215705, 2009.

[10] Rogers R. C. A study of the mixing of hydrogen injected normal to a supersonic airstream //NASA TN D-6114, 1971

Yekaterina Moisseyeva, Al-Farabi Kazakh National University, Almaty, Kazakhstan
Altynshash Naimanova, Institute of Mathematics and Mathematical Modelling, Almaty, Kazakhstan